The N-Terminal Subdomain of Insulin-like Growth Factor (IGF) Binding Protein 6. Structure and Interaction with IGFs†

Indu R. Chandrashekaran,‡ Shenggen Yao,‡ Chunxiao C. Wang,‡,§ Paramjit S. Bansal,|| Paul F. Alewood,|| Briony E. Forbes,⊥ John C. Wallace,⊥ Leon A. Bach,# and Raymond S. Norton*,‡

The Walter and Eliza Hall Institute of Medical Research, 1G Royal Parade, Parkville 3050, Australia, Institute for Molecular Bioscience, University of Queensland, Queensland 4072, Australia, School of Molecular and Biomedical Science, University of Adelaide, Adelaide 5005, Australia, and Department of Medicine, Monash University, and Department of Endocrinology and Diabetes, Alfred Hospital, Melbourne 3004, Australia

Received September 25, 2006; Revised Manuscript Received December 15, 2006

ABSTRACT: Insulin-like growth factor binding proteins (IGFBPs) modulate the activity and distribution of insulin-like growth factors (IGFs). IGFBP-6 differs from other IGFBPs in being a relatively specific inhibitor of IGF-II actions. Another distinctive feature of IGFBP-6 is its unique N-terminal disulfide linkages; the N-domains of IGFBPs 1−5 contain six disulfides and share a conserved GCGCC motif, but IGFBP-6 lacks the two adjacent cysteines in this motif, so its first three N-terminal disulfide linkages differ from those of the other IGFBPs. The contributions of the N- and C-domains of IGFBP-6 to its IGF binding properties and their structure−function relationships have been characterized in part, but the structure and function of the distinctive N-terminal subdomain of IGFBP-6 are unknown. Here we report the solution structure of a polypeptide corresponding to residues 1−45 of the N-terminal subdomain of IGFBP-6 (NN-BP-6). The extended structure of the N-terminal subdomain of IGFBP-6 is very different from that of the short two-stranded β-sheet of the N-terminal subdomain of IGFBP-4 and, by implication, the other IGFBPs. NN-BP-6 contains a potential cation-binding motif; lanthanide ion binding was observed, but no significant interaction was found with physiologically relevant metal ions like calcium or magnesium. However, this subdomain of IGFBP-6 has a higher affinity for IGF-II than IGF-I, suggesting that it may contribute to the marked IGF-II binding preference of IGFBP-6. The extended structure and flexibility of this subdomain of IGFBP-6 could play a role in enhancing the rate of ligand association and thereby be significant in IGF recognition.

Insulin-like growth factors (IGFs)[1] are potent mitogens that promote cell proliferation, differentiation, and survival and are therefore essential for normal mammalian growth and development. As aberrant regulation of the IGF system is implicated in many diseases, including cancer, diabetes, and atherosclerosis, there is considerable interest in the development of IGF-based therapeutics for these diseases (*1*, *2*). A family of six structurally related high-affinity IGF binding proteins (IGFBPs) regulates the activity of the IGFs by modulating their availability to the IGF receptors (*3*). IGFBPs act as carrier proteins for IGFs in interstitial and extracellular fluids and help to maintain a reservoir of IGFs. The affinity of IGFBPs for IGFs is regulated by several mechanisms including proteolysis, phosphorylation, and binding to the extracellular matrix (*4*).

IGFBP-6 is distinct from other IGFBPs in having a marked binding preference for IGF-II, as it binds IGF-II with 20−100-fold higher affinity than IGF-I (*5*). IGFBP-6 is a relatively specific IGF-II inhibitor and has been found to inhibit growth of a number of IGF-II-dependent cancers, including rhabdomyosarcoma, neuroblastoma, and colon cancer (*5*). Therapeutics based on IGFBP-6 may be advantageous for IGF-II-dependent tumors in children as they would not interfere with IGF-I-dependent growth.

All IGFBPs share a common three-domain organization (*6*). The N- and C-terminal domains exhibit high amino acid sequence identity across the six IGFBPs and contain conserved intradomain disulfide bonds, except for the N-domain of IGFBP-6. The conserved N- and C-domains each contribute to high-affinity IGF binding. These domains are joined by a variable "linker" domain which is not directly involved in high-affinity IGF binding. IGFBP-6 lacks two conserved cysteines in the N-terminal domain and therefore

†This work was supported in part by an Australian Research Council Discovery Grant (DP0449906).

* To whom correspondence should be addressed. E-mail: ray.norton@wehi.edu.au. Fax: +61 3 9345 2686. Phone: +61 3 9345 2306.

‡ The Walter and Eliza Hall Institute of Medical Research.

§ Present address: Department of Biochemistry and Molecular Biology, Monash University, Clayton 3800, Australia.

|| University of Queensland.

⊥ University of Adelaide.

Monash University.

[1] Abbreviations: C-BP-6, C-terminal domain of insulin-like growth factor binding protein 6; C-BP-4, C-terminal domain of insulin-like growth factor binding protein 4; HPLC, high-pressure liquid chromatography; HSQC, heteronuclear single-quantum coherence; IGF, insulin-like growth factor; IGFBP, insulin-like growth factor binding protein; LC-MS, liquid chromatography−mass spectrometry; NMR, nuclear magnetic resonance; N-BP-4, N-terminal domain of insulin-like growth factor binding protein 4; NN-BP-6, N-terminal subdomain of insulin-like growth factor binding protein 6; NOE, nuclear Overhauser effect; SPPS, solid-phase peptide synthesis.

10.1021/bi0619876 CCC: $37.00
Published on Web 02/17/2007

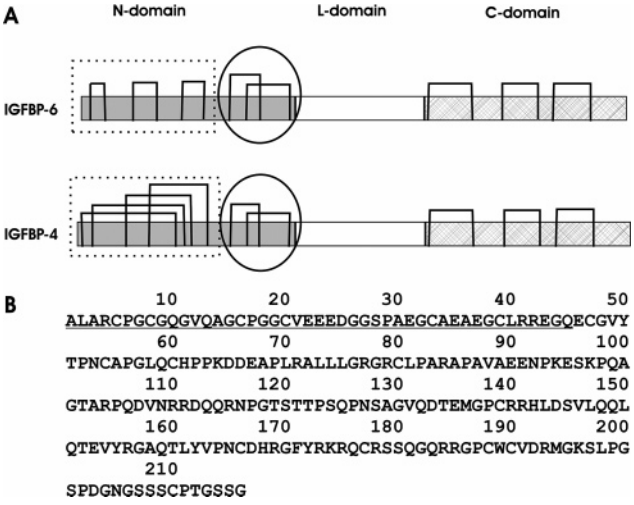

FIGURE 1: (A) Comparison of domain structures of IGFBP-6 and IGFBP-4. The disulfide bonds in the N- and C-domains are shown as vertical lines joined by horizontal lines. The N-domain is subdivided into the N-terminal subdomain (NN-BP-6, shown as dashed boxes) and the mini-BP domain (highlighted by circles). (B) Amino acid sequence of IGFBP-6 with the N-terminal subdomain underlined.

differs from other IGFBPs in its N-terminal disulfide linkages (Figure 1A) (*7*). The unique disulfide linkages of the N-terminal subdomain of IGFBP-6 could result in a different fold which, in turn, could contribute to the distinctive IGF binding characteristics of IGFBP-6.

Although the structure of a full-length IGFBP has not yet been determined, there have been several reports of structural characterization of individual domains of IGFBPs. The three-dimensional structures of the region containing residues 40−92 of the N-domain of IGFBP-5 (mini-BP-5) (*8*) and the complete C-domain of IGFBP-6 have been solved by NMR (*9*). Mini-BP-5 adopts a compact structure consisting of a three-stranded β-sheet and a short α-helix stabilized by two disulfide bonds (*8*). The C-domain of IGFBP-6 adopts a thyroglobulin type 1 fold in its proximal region, which consists of an α-helix followed by a three-stranded antiparallel β-sheet stabilized by two disulfide bonds, while the distal region consists of a flexible loop constrained only by the third disulfide bond (*9*). The crystal structure of the C-terminal domain of IGFBP-1 was solved recently (*10*), and more recently, the solution structure of the C-terminal domain of IGFBP-2 was solved by NMR (*11*). Both of these domains were found to adopt a thyroglobulin type 1 fold similar to that of C-BP-6 (*9*). The crystal structure of the N-terminal domain of IGFBP-4 in complex with IGF-I has been reported (*12*), and more recently, the structure of the ternary complex of N-BP-4/IGF-I/C-BP-4 was also reported (*13*). The N-terminal subdomain of IGFBP-4 (residues 1−39) adopts a novel fold stabilized by a short two-stranded β-sheet and four disulfide bridges, forming a disulfide bond ladder-like structure. The primary IGF-I binding site of N-BP-4 was similar to that of mini-BP-5 (*14*), although, contrary to previous reports on IGFBP-5 (*8*), the N-terminal subdomain of IGFBP-4 made additional contacts with IGF-I. N-BP-4 binds IGF-I with 4−5-fold higher affinity than mini-BP-4 (residues 40−83) (*12*), and the extra contacts observed between IGF-I and N-BP-4 involving hydrophobic residues of the N-terminal subdomain of IGFBP-4 may account for this increased affinity, since removal of these residues reduced IGF-I binding 10-fold (*13*). The hydrophobic residues in the "thumb" region (residues 1−5) of the N-terminal subdomain of IGFBP-4 mask the IGF residues responsible for IGF-IR binding and may play an important role in inhibiting IGF-induced autophosphorylation of the IGF-IR (*12*). In the crystal structure of the ternary complex of N-BP-4/IGF-I/C-BP-4, the C-terminal domain was found to be close to the N-terminal subdomain and interacted extensively with its thumb region, thus stabilizing the complex and contributing to blocking the IGF-IR binding region of IGF-I (*13*).

As the N-terminal subdomain of IGFBP-6 (residues 1−45) has distinct disulfide connectivities from those of the other five IGFBPs, it was of interest to determine its structure and possible contribution to the distinctive IGF binding characteristics of IGFBP-6. In this study we have determined the solution structure of a polypeptide corresponding to the N-terminal subdomain of IGFBP-6 (*1*−*45*), designated NN-BP-6 (Figure 1B), using NMR spectroscopy. NN-BP-6 contains a potential cation-binding site in its sequence (Glu22-Asp25) which is unique to IGFBP-6. Moreover, cations have also been reported to modulate the affinity of IGFBPs for IGFs (*15*, *16*), so the interactions of metal ions with the peptide were monitored using NMR. The interactions of this subdomain of IGFBP-6 with IGF-I and IGF-II were then investigated using NMR.

MATERIALS AND METHODS

Peptide Synthesis. A peptide corresponding to NN-BP-6 was synthesized as two separate segments using SPPS methodology and ligated through native chemical ligation. The two segments corresponding to residues 1−19 and 20−45 were synthesized separately, purified by HPLC, and characterized by mass spectrometry. Ligation of the N-terminal segment thioester and the C-terminal segment was carried out in phosphate buffer at pH 7.5. 2-Mercaptoethanesulfonic acid sodium salt (0.2%) was added to an equivalent mixture of the two peptide segments in phosphate buffer, and the mixture was vortexed. The reaction was monitored at regular time intervals by HPLC. The ligation reaction was complete in 1 h, following which the reaction was quenched with 5% TFA, and the peptide was purified by HPLC and characterized by mass spectrometry (Figure S1, Supporting Information). The purified peptide was folded under oxidizing conditions, and the disulfide connectivities were confirmed by enzymatic hydrolysis with endoproteinase Glu-C and analyzed by LC-MS.

NMR Spectroscopy and Structure Determination. Samples were prepared for NMR by dissolving lyophilized NN-BP-6 in 10 mM sodium acetate buffer (95% H_2O, 5% ^2H_2O) to a final concentration of 1.1 mM at a pH of 4.3. Two-dimensional homonuclear TOCSY, DQF-COSY, and NOESY spectra were recorded for the peptide at 288 K on Bruker DRX 600 and Avance 800 spectrometers. NOESY spectra were recorded for the peptide at mixing times of 50, 100, 250, and 300 ms. $^1H-^{13}C$ HMQC spectra for the assignment of ^{13}C chemical shifts (*17*) and a $^1H-^{15}N$ HSQC spectrum for the assignment of ^{15}N chemical shifts (*18*) were collected on a natural abundance sample of NN-BP-6 on a Bruker Avance 500 spectrometer equipped with a cryoprobe. To monitor backbone amide exchange, a series of 1D spectra was recorded at various time intervals for the sample in

100% ^2H_2O at 288 K at 600 MHz. Diffusion measurements were performed using a PFG longitudinal eddy-current delay pulse sequence (*19*). The interactions of NN-BP-6 with lanthanide and calcium ions were investigated by recording a series of ^1H 1D spectra and 2D TOCSY spectra on a Bruker Avance 500 spectrometer at NN-BP-6:Yb^{3+} ion ratios of 1:0.5, 1:1, 1:2, 1:3, and 1:4 and NN-BP-6:Ca^{2+} ratios of 1:1, 1:2, 1:4, 1:6, 1:8, and 1:10 at 288 and 293 K, respectively. Interactions of NN-BP-6 with magnesium and ferric ions were also investigated by recording a series of 1D spectra at NN-BP-6:Fe^{3+} and NN-BP-6:Mg^{2+} ion ratios of 1:1, 1:5, and 1:10. The interactions of NN-BP-6 with cations were studied at different pH values in the range 4.3−6.3. Spectra were referenced to an impurity peak at 0.15 ppm and/or dioxane at 3.75 ppm (*20*). Spectra were processed using XWINNMR version 3.5 (Bruker Biospin) or TopSpin version 1.3 and analyzed using XEASY version 1.3 (*21*).

Structures for the peptide were calculated using distance restraints from 2D NOESY spectra (250 ms) acquired at 600 MHz. $^3J_{HNH\alpha}$ values were measured from a DQF-COSY spectrum, and the apparent coupling constants were corrected for the effect of the line width using in-house software. $^3J_{HNH\alpha}$ values were converted to φ dihedral restraints as follows: $^3J_{HNH\alpha} > 8$ Hz, $\varphi = -120 \pm 30°$; $^3J_{HNH\alpha} < 6$ Hz, $\varphi = -60 \pm 30°$. Intensities of NOE cross-peaks measured in XEASY were calibrated using the CALIBA macro from the program CYANA (*22*). Initial structures were calculated using torsion angle dynamics and simulated annealing protocols in CYANA, and structures were optimized for a low target function. The final constraint set was then used to calculate a new family of 200 structures using X-PLOR-NIH (*23*). The 50 lowest energy structures were further refined in a shell of water molecules using the simulated annealing protocol in X-PLOR-NIH (*23*). A final family of 20 lowest energy structures was chosen for analysis using PROCHECK-NMR (*24*) and MOLMOL (*25*). Structural figures were prepared using MOLMOL and PyMol (http://www.pymol.org).

Interaction with IGF-I and -II. To investigate the interactions of NN-BP-6 with IGF-I and IGF-II, $^{15}N-^1H$ HSQC spectra of 0.1 mM ^{15}N-labeled IGF-I in 10 mM sodium acetate (95% H_2O, 5% ^2H_2O) at pH 6.0 and 0.12 mM ^{15}N-labeled IGF-II in 10 mM sodium acetate (95% H_2O, 5% ^2H_2O) at pH 4.1 were recorded, respectively, in the presence and absence of unlabeled NN-BP-6. The latter pH was chosen since IGF-II spectra at higher pHs are of poor quality due to significant line broadening, which has been attributed to oligomerization and/or conformational exchange (*26*, *27*). All spectra were recorded at 298 K on a Bruker Avance 500 spectrometer equipped with a cryoprobe. A series of two-dimensional $^{15}N-^1H$ HSQC spectra was recorded at IGF-II:NN-BP-6 ratios of 1:0.5, 1:1, 1:1.5, and 1:2 and IGF-I:NN-BP-6 ratios of 1:0.5, 1:1, 1:2, 1:3, and 1:4. ^{15}N double half-filtered NOESY (*28*) spectra were recorded for unlabeled NN-BP-6 in the presence of ^{15}N-labeled IGF-II at IGF-II:NN-BP-6 ratios of 1:1 and 1:2.

The average chemical shift deviations for the perturbed IGF-I peaks were computed using the formula $\Delta\delta_{av} = ([^1/_2[(\Delta\delta_H)^2 + (0.2\ \Delta\delta_N)^2]])^{1/2}$, where $\Delta\delta_H$ and $\Delta\delta_N$ denote the chemical shift changes (in parts per million) of the amide hydrogen and nitrogen, respectively (*29*). The average chemical shift was plotted as a function of the molar ratio of IGF-I to NN-BP-6 for the four significantly perturbed peaks. The titration curves were fitted using nonlinear regression assuming a single binding site saturation using the program Sigmaplot 8.0 (SPSS Inc.), and the average apparent K_d for the interaction of IGF-I and NN-BP-6 was determined.

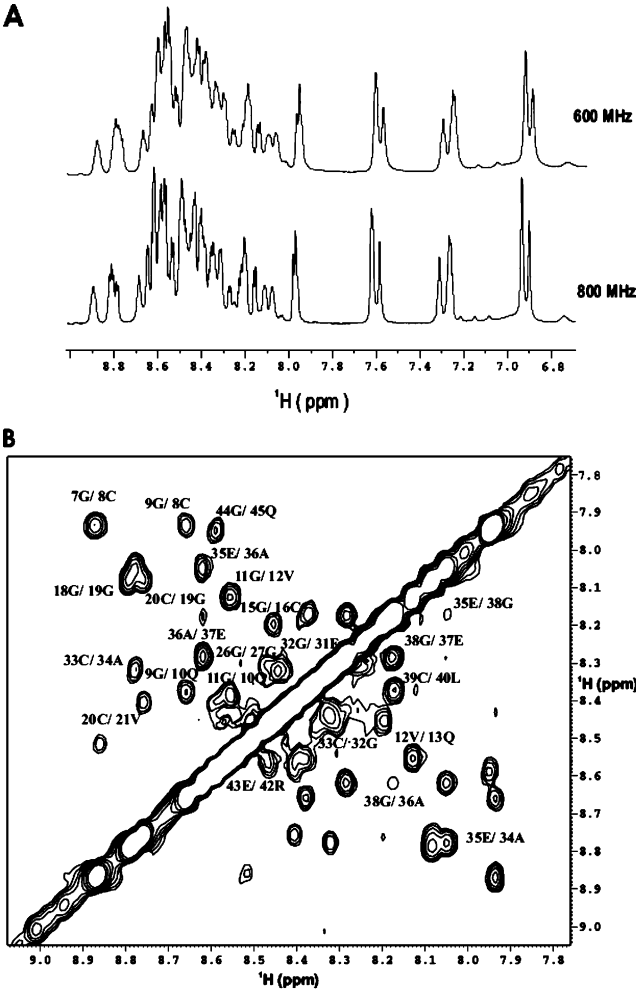

FIGURE 2: (A) Amide region of the ^1H 1D spectra of NN-BP-6 recorded at 288 K and pH 4.3 on 600 and 800 MHz spectrometers. (B) NH−NH region of the NOESY spectrum of NN-BP-6, recorded at 288 K, pH 4.3, and 600 MHz.

RESULTS

Peptide Synthesis. The peptide corresponding to NN-BP-6 consists of 45 amino acids (Figure 1B). It was synthesized as two separate segments using SPPS methodology and ligated by native chemical ligation. The purified peptide was folded to give the required product containing consecutive disulfide bonds and was characterized by mass spectrometry (Figure S1, Supporting Information). The disulfide connectivities were confirmed by enzymatic hydrolysis of the peptide with endoproteinase Glu-C and analysis by LC-MS (Figure S2, Supporting Information). Five fragments were detected; the major cleavage fragments were consistent with alternate Glu-C cleavages in the sequence EEED, and minor fragments were due to cleavages at other Glu residues.

Structure of the N-Terminal Subdomain of IGFBP-6. ^1H NMR spectra of NN-BP-6 were characterized by limited chemical shift dispersion (Figure 2A). ^1H spectra recorded at 800 MHz showed no significant improvement in dispersion

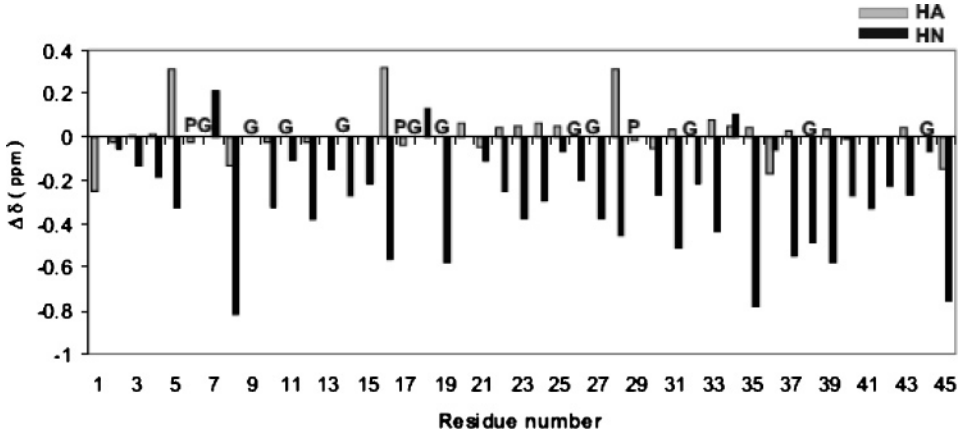

FIGURE 3: Deviation of chemical shifts from random coil values. Chemical shift deviations for $C^{\alpha}H$ and backbone amides of NN-BP-6 were compared to the random coil chemical shifts of Merutka et al. (*46*). The letters G and P indicate glycine and proline residues, respectively.

(Figure 2A). 1D and 2D spectra were recorded at different temperatures and pH values in the range 3.3−6.3 in an effort to improve spectral dispersion. This was optimal at 288 K and pH 4.3. pH 4.3 was chosen for the NMR experiments to minimize the exchange of labile protons that occurs at higher pH. Moreover, a similar set of NOEs was observed for the peptide at pH 6.3, which is close to physiological pH, confirming that there was no significant change in structure over this pH range. ^{1}H chemical shifts were assigned for all backbone and most side chain protons (Table S1, Supporting Information), and ^{15}N and ^{13}C chemical shifts were assigned for most backbone amides and C^{α} carbons, respectively. The assignments have been deposited in the BioMagResBank database (accession no. 7262). The peptide contains three prolines, all of which were found to adopt predominantly a *trans* conformation. However, a few minor peaks were observed in the spectra, which could be attributed to minor amounts of *cis*-proline conformers. The disulfide bond connectivities Cys5−Cys8, Cys16−Cys20, and Cys33−Cys36 were supported by characteristic $C^{\beta}H/C^{\beta}H$ and $C^{\alpha}H/C^{\beta}H$ NOEs observed for disulfide pairs (*30*). Translational diffusion coefficients were measured for the peptide at various temperatures and pHs. The diffusion coefficient for NN-BP-6 at 288 K and pH 4.3 was $1.48 \pm 0.01 \times 10^{-10}$ m^2/s (SD over 14 resonances of the peptide). The translational diffusion coefficients of NN-BP-6 and other peptides under different solution conditions were compared (Table S2, Supporting Information); allowing for viscosity and temperature effects these values were similar (*19*, *31*, *32*), implying that NN-BP-6 was monomeric. The relatively small deviations of $C^{\alpha}H$ and backbone amide chemical shifts from random coil values indicated the absence of a well-defined secondary structure in the peptide (Figure 3).

Structures were calculated using distance restraints obtained from two-dimensional homonuclear NOESY spectra. A summary of the medium-range, sequential, and intraresidue NOEs and dihedral restraints used in the final calculations in CYANA and X-PLOR is given in Table 1. Very few medium-range NOEs and no long-range NOEs ($i - j > 4$) were observed for the peptide, confirming that it lacked a well-defined structure in solution (Figure 2B and Figure S3, Supporting information). A series of amide exchange experiments indicated the absence of slowly exchanging protons, and no amide temperature coefficients ($\Delta\delta/\Delta T$) with magnitude <5.6 ppb/K were observed, so no hydrogen bond restraints were included in the structure calculations. The structural statistics for the final family of 20 structures of NN-BP-6 are listed in Table 1. No distance violations >0.2 Å or dihedral violations >5° were observed in the final structures. The structures have been deposited in the Protein Data Bank (PDB ID 2JM2).

Table 1: Structure Statistics for NN-BP-6

no. of distance restraints	428
intraresidue ($i = j$)	240
sequential ($\|i - j\| = 1$)	154
medium range ($1 < \|i - j\| < 5$)	34
no. of dihedral restraints	18
E_{NOE} (kcal/mol)	15.61 ± 3.0
deviations from experimental data	
NOEs (Å)	0.036 ± 0.04
dihedrals (deg)	0.48 ± 0.18
deviations from ideal geometry[a]	
bonds (Å)	0.0045 ± 0.0002
angles (deg)	0.63 ± 0.02
impropers (deg)	0.43 ± 0.02
RMSD (Å),[b] residues 20−22	
all heavy atoms	1.66
backbone heavy atoms	0.69
RMSD (Å),[b] residues 33−37	
all heavy atoms	1.95
backbone heavy atoms	0.86
Ramachandran plot[c]	
most favored (%)	41.6
allowed (%)	52.2
additionally allowed (%)	6.2
disallowed (%)	0

[a] The values for the bonds, angles, and impropers show the deviations from ideal values based on perfect stereochemistry. [b] The mean pairwise RMSD over the backbone and all heavy atoms (N, C^{α}, C) over the well-ordered residues ($S_{\varphi,\psi} > 0.8$). [c] As determined by the program PROCHECK-NMR for all residues except Gly and Pro.

The angular order parameter S was used to assess the precision of torsion angles within an ensemble of structures. The φ and ψ angles were generally well ordered ($S \geq 0.8$) over residues 20−22 and 33−37 (Figure S4, Supporting Information). The decrease in angular order parameters for the other residues of the peptide was reflected in the greater disorder observed in the family of structures. The global structure of the peptide was not well defined, with the mean pairwise RMSD over the backbone heavy atoms (N, C^{α}, C) of the entire peptide being 7.9 Å. However, the local structure was apparent in the regions proximal to the disulfide bridges (Figure 4). The closest-to-average structure is shown in Figure

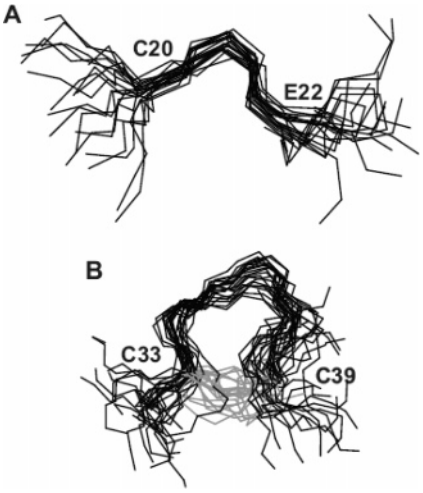

FIGURE 4: Ensemble of 20 structures showing the structured regions of NN-BP-6. Structures were superimposed over the backbone heavy atoms (N, C^{α}, C) of (A) residues 20−22 (RMSD 0.69 Å) and (B) residues 33−37 (RMSD 0.86 Å). Disulfide linkages between residues 33−39 are shown in gray for the ensemble. The poorly defined regions of the peptide are not included in the figure for improved clarity.

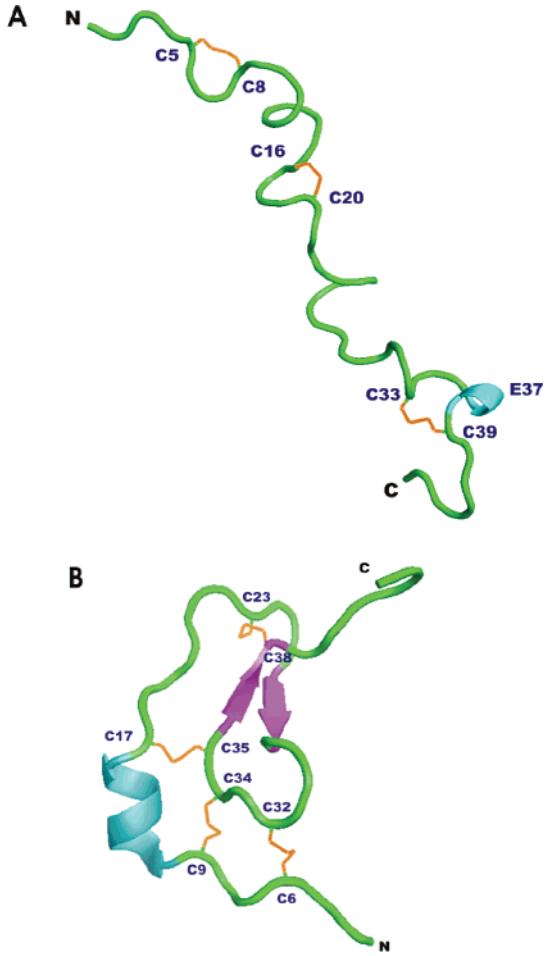

FIGURE 5: Comparison of (A) the closest-to-average NMR structure of NN-BP-6 with (B) the crystal structure of NN-BP-4 (PDB ID 1WQJ). The disulfide linkages are highlighted in orange in both structures.

5A. The peptide adopts an extended structure along its entire length except in the region from residue 36 to residue 39, where it has a turn of α-helix.

Interaction of NN-BP-6 with Cations. NN-BP-6 has a stretch of negatively charged residues (*22*−*25*) in its sequence which represents a potential cation-binding site. This motif of negatively charged residues is not present in the N-terminal subdomains of other IGFBPs and appears to be an insertion in IGFBP-6. Paramagnetic lanthanide ions are widely employed as NMR probes for cation-binding proteins as they have ionic radii (0.85−1.1 Å) similar to those of calcium ions and similar coordination chemistry (*33*, *34*). The interaction with paramagnetic lanthanide ions affects the properties of nuclear spins in their vicinity and causes peaks within a certain distance from the metal center to be broadened beyond detection and those outside this shell to be shifted (*35*). Addition of paramagnetic Yb^{3+} led to line broadening and the subsequent disappearance of several resonances of NN-BP-6. Peaks corresponding to Gln13, Glu23, Asp25, Ser28, Glu31, Glu35, and Glu37 disappeared at a Yb^{3+}:NN-BP-6 ratio of 3:1 (Figure S5, Supporting Information), implying that these residues form a metal-binding site. These results indicate specific interactions of the lanthanide ion with the peptide; generalized broadening due to nonspecific binding was not observed. We then investigated the interaction of NN-BP-6 with Ca^{2+} ions. NMR spectra were recorded at various peptide to Ca^{2+} ratios, but no significant changes in the spectra were observed with ratios below 1:10. At a 1:10 ratio, slight shifts were observed for the peaks corresponding to the side chain protons of Glu23, Glu24, Glu31, and Glu35 (Figure S6A, Supporting Information). These residues form a continuous surface when mapped onto the structure of NN-BP-6, implying specific interactions (Figure S6B, Supporting Information). However, it can be inferred that the peptide did not interact significantly with Ca^{2+} ions over the pH range of 4.3−6.3, and the weak interactions observed at high Ca^{2+} concentrations are unlikely to be of physiological relevance (although it should be noted that there is a 100-fold excess of extracellular Ca^{2+} ions compared to circulating IGFBP-6). No evidence of structural ordering of NN-BP-6 was observed in the presence of calcium. Interactions of NN-BP-6 with $Mg^{2+}$and Fe^{3+} ions were also studied, but no significant changes were observed in the spectra even at NN-BP-6:Mg^{2+} and NN-BP-6:Fe^{3+} ratios of 1:10, indicating that this region of IGFBP-6 did not bind strongly to either of these metal ions (data not shown).

Interaction of NN-BP-6 with IGF-I and -II. Unambiguous assignments were made for most of the cross-peaks in the $^{15}N-^{1}H$ HSQC spectrum of free IGF-I and -II based on published chemical shifts (*26*, *36*). The residues affected by NN-BP-6 binding were identified from changes in $^{15}N-^{1}H$ HSQC spectra of ^{15}N-labeled IGF-I and -II upon addition of unlabeled NN-BP-6.

Upon addition of unlabeled NN-BP-6 to ^{15}N-labeled IGF-II, several resonances showed line broadening and subsequently disappeared, implying intermediate exchange between the free and bound forms and a K_d in the micromolar range (Figure 6A). The largest decreases in backbone cross-peak intensities were observed for the IGF-II residues Gly10, Gly11, Leu13, Leu17, Val20, Gly25, Phe 26, Tyr27, Phe28, Cys46, and Phe48 (Figure 6A). Their $^{15}N-^{1}H$ HSQC peaks showed a decrease in cross-peak intensity due to line broadening at IGF-II:NN-BP-6 ratios of 1:1 (Figure S7,

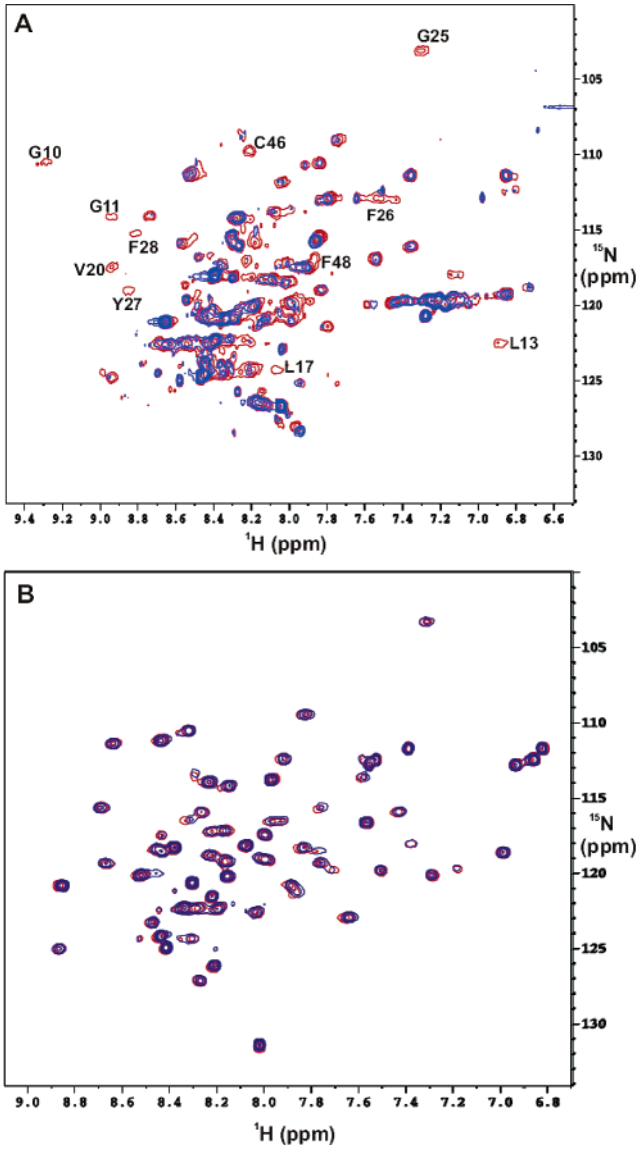

FIGURE 6: Comparison of ^{1}H−^{15}N HSQC of (A) ^{15}N-labeled IGF-II in the absence (red) and presence (blue) of NN-BP-6 (IGF-II:NN-BP-6, 1:2) (the IGF-II residues most affected by NN-BP-6 binding are labeled) and (B) ^{15}N-labeled IGF-I in the absence (red) and presence (blue) of NN-BP-6 (IGF-I:NN-BP-6, 1:1). Spectra were recorded at 298 K and 500 MHz at pH 4.1 and 6.0, respectively. The free and ligand-bound spectra are plotted at the same levels.

Supporting information) and subsequently disappeared at IGF-II:NN-BP-6 ratios of 1:2 (Figure 6A).

Decreases in cross-peak intensity were observed only for those peaks corresponding to residues highlighted in Figure 7A. Hence, it can be concluded that the disappearance of resonances was due to chemical exchange of the bound and the free forms and not a result of nonspecific line broadening. We note that binding interfaces identified by mapping chemical shift perturbations are usually larger than those obtained from X-ray crystallographic studies (*37*, *38*), so the actual binding interface between NN-BP-6 and IGF-II may be smaller than the surface represented in Figure 7A.

In contrast to its effects on the ^{15}N−^{1}H HSQC spectrum of IGF-II, the chemical shift perturbations upon addition of unlabeled NN-BP-6 to ^{15}N-labeled IGF-I were small. A set of peaks was consistently perturbed, but only slightly, indicating fast exchange between the free and bound forms and in turn implying weak interaction between NN-BP-6 and IGF-I (Figure 6B). In the case of fast exchange, the observed chemical shifts are a population-weighted average of the bound and unbound forms (*39*). By fitting the titration curves of the significantly perturbed peaks of IGF-I residues Thr4, Phe23, Leu54, and Arg56, we calculated an average apparent K_d of 3.3 ± 1.9 mM, indicating very weak affinity of NN-BP-6 for IGF-I (Figure S8, Supporting Information).

A ^{15}N double half-filtered NOESY spectrum was recorded for unlabeled NN-BP-6 in the presence of ^{15}N-labeled IGF-II to monitor any change in conformation induced in NN-BP-6 upon IGF-II binding. Slight chemical shift changes (<0.02 ppm) were observed for some of the NN-BP-6 resonances (Gly7, Gly9, Cys16, Cys20, Ala34, Glu35, and Glu37) on binding to IGF-II. The lack of significant chemical shift changes indicates that NN-BP-6 does not undergo any major conformational change upon binding IGF-II. However, several additional NOE cross-peaks, probably arising from intermolecular NOEs with IGF-II, were observed in the spectrum (Figure 8). We believe that these additional NOEs are inter- rather than intramolecular as they do not correspond exactly to chemical shifts in NN-BP-6, but this remains to be confirmed.

Translational diffusion coefficients were measured for IGF-II in the presence and absence of NN-BP-6. The diffusion coefficient for IGF-II in the presence of NN-BP-6 (IGF-II:NN-BP-6, 1:1) was 1.34 ± 0.03 × 10^{-10} m^2/s (SD over 16 resonances of the IGF-II), and the value for free IGF-II was 1.62 ± 0.02 × 10^{-10} m^2/s (SD over 16 resonances of the IGF-II). The slower diffusion of IGF-II in the presence of NN-BP-6 is consistent with formation of an IGF-II/NN-BP-6 complex.

DISCUSSION

IGFBP-6 lacks two conserved N-terminal cysteines, and its N-terminal disulfide linkages differ from those of the other IGFBPs (*7*). Using NMR spectroscopy, we have determined that the N-terminal subdomain of IGFBP-6 adopts an extended structure (Figure 5A), which differs markedly from the short two-stranded β-sheet of the equivalent subdomain of IGFBP-4 (Figure 5B) (*12*). The structure of the N-terminal subdomain of IGFBP-4 is stabilized by four disulfide bridges that form a ladder-like structure (Figure 5B), while the disulfide bridges in NN-BP-6 are consecutive and less constraining (Figure 5A). The difference in structures could therefore be attributed to the different disulfide linkages present in the N-terminal subdomain of IGFBP-6 in comparison to other IGFBPs. However, there are two other possibilities that need to be considered.

The first of these is interdomain interactions. The IGFBP-4 N-terminal subdomain structure was determined as part of a ternary complex involving the entire N-domain, the C-domain, and IGF-I (*12*). The mini-BP-4 domain, which is stabilized by the two disulfide linkages that are conserved across the entire IGFBP family, as shown in Figure 1A, was found to make extensive interactions with the N-terminal subdomain of IGFBP-4 (*12*). A network of hydrogen bonds is formed between Arg50 and Ser53 of mini-BP-4 and Glu23, Glu27, and Glu29 of NN-BP-4, which contributes to a high degree of rigidity of the entire N-domain of IGFBP-4. The thumb region of NN-BP-4 (residues 1−5) interacts exten-

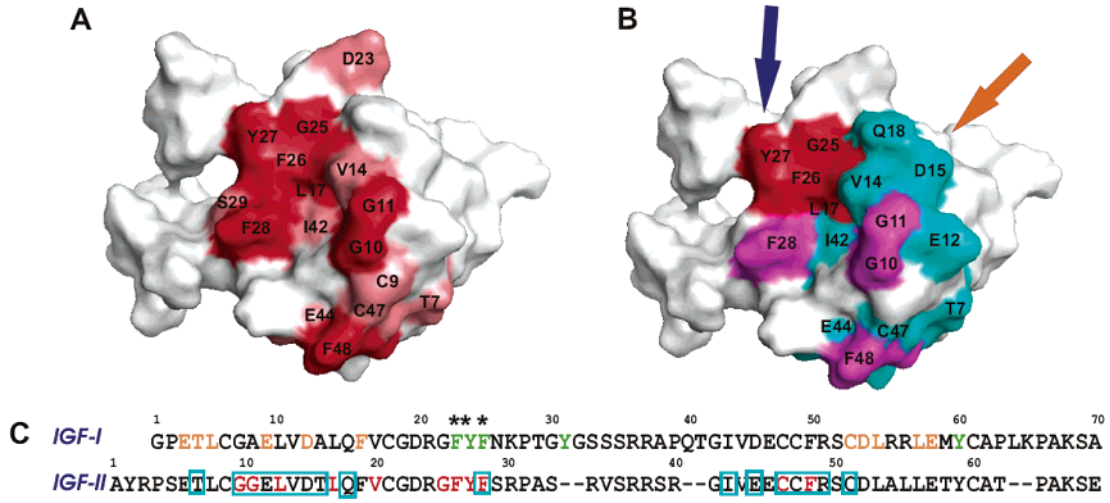

FIGURE 7: Surface representation of the closest-to-average NMR structure of IGF-II (PDB ID 1IGL) (*26*) showing residues involved in NN-BP-6 binding. (A) Binding site of NN-BP-6, with the residues most affected by binding shown in red and those affected slightly shown in salmon. Three residues whose backbone amide resonances disappeared in Figure 6A, i.e., Leu13, Val20, and Cys46, are not visible in this view of the structure; Leu13 and Cys46 are buried, and Val20 is on the opposite face. (B) Comparison of binding sites of C-BP-6 (cyan) and NN-BP-6 (residues most affected by IGF-II binding) (red). Binding residues common to both domains are highlighted in magenta. The binding sites for IGF-IR and mini-BP-5 (*8*) are indicated by dark blue and orange arrows, respectively. (C) Sequence alignment of IGFs showing the binding sites for IGFBPs. Residues that interact with mini-BP-5 (*8*) are highlighted in orange, those that interact with IGF-IR are in green, those that interact with NN-BP-6 are in red (this work), and those that interact with C-BP-6 (*27*) are in the cyan box. IGF-I residues that makes contact with NN-BP-4 (*12*) are marked with asterisks.

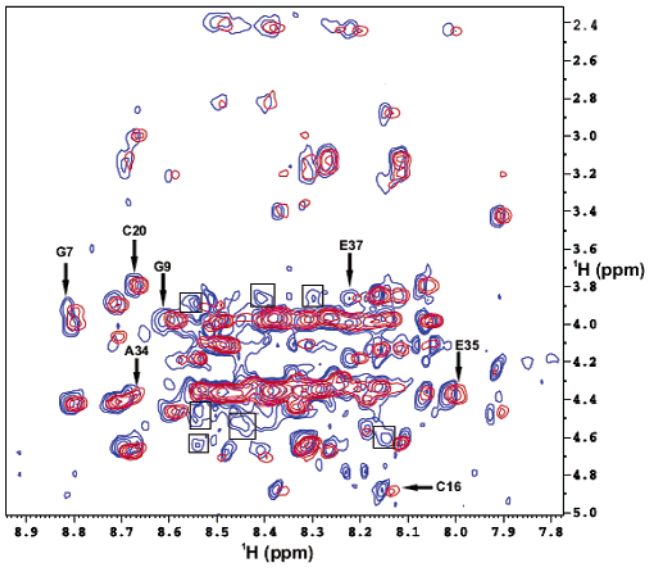

FIGURE 8: Overlay of the ^{15}N double half-filtered NOESY of NN-BP-6:IGF-II (1:1) (blue) with the 2D ^{1}H−^{1}H NOESY of free NN-BP-6 (red). The spectra were recorded at pH 4.0, 298 K, and 500 MHz. NN-BP-6 resonances that undergo slight chemical shift perturbation upon binding IGF-II are indicated by arrows and labeled. Cross-peaks probably arising from intermolecular NOEs with IGF-II are highlighted in black squares. Two cross-peaks around 4.78 ppm in the blue spectrum coincide with the water resonance and probably arise from chemical exchange with water.

sively with the C-BP-4 domain (segment between residues 168 and 173), and the segments form a short parallel-like β-sheet stabilized by interdomain hydrogen bonds (*13*). Thus, it is possible that these interdomain interactions alter the structure of the NN-BP-4. In order to address whether this may be the case for NN-BP-6, we compared the ^{1}H−^{15}N HSQC spectra of NN-BP-6 and full-length IGFBP-6 (Figure S9, Supporting Information). It is clear that the majority of resonances in NN-BP-6 can be readily matched with corresponding resonances in the full-length protein, except for Gln45, which is the C-terminal residue and thus is expected to have a different chemical shift (the NN-BP-6 sample was not amidated). As assignments for full-length IGFBP-6 are not available, it cannot be confirmed that resonances with the same chemical shift arise from the same backbone amide, but the excellent match implies that the NN-BP-6 resonances are not perturbed in the full-length protein, and this, in turn, implies that the NN-BP-6 structure is also not affected by the rest of the protein.

As the structure of the N-terminal subdomain of IGFBP-4 was determined in complex with IGF-I, it is possible that IGF-I induced structural changes in this domain. NN-BP-6 binds preferentially to IGF-II, so in order to investigate any possible "induced folding" of NN-BP-6 on binding to IGF-II, a ^{15}N double half-filtered NOESY (*28*) was recorded for the unlabeled NN-BP-6 in the presence of ^{15}N-labeled IGF-II. Data from this experiment suggest a lack of any significant structural change in NN-BP-6 on binding to IGF-II (Figure 8), which is contrary to expectations. However, there is increasing evidence that a protein can function in an unstructured state (*40*, *41*), and the conformations of disordered domains of some proteins have been reported to remain unchanged upon ligand binding (*42*).

To explore possible IGF interactions with NN-BP-6, the effects of NN-BP-6 on the spectra of ^{15}N-labeled IGF-I and IGF-II were investigated. The binding of NN-BP-6 to IGF-I was found to be weak and resulted in only small chemical shift perturbations in the ^{1}H−^{15}N HSQC spectra of IGF-I. An average apparent K_d of 3.3 ± 1.9 mM was calculated from the binding isotherm, indicating low affinity of NN-BP-6 for IGF-I. In contrast, ^{1}H−^{15}N HSQC spectra of IGF-II in the presence of NN-BP-6 showed intermediate exchange, resulting in the disappearance of several peaks. Moreover, several putative intermolecular NOE cross-peaks with IGF-II were observed in the ^{15}N double half-filtered

NOESY, confirming the NN-BP-6/IGF-II interaction. This implies that the N-terminal subdomain has greater affinity for IGF-II than IGF-I and thus may contribute to the marked IGF-II binding preference of IGFBP-6. Although NN-BP-6 binds IGF-I with low affinity, the resonances perturbed by binding were equivalent to those in IGF-II. When the residues affected by NN-BP-6 were mapped onto the solution structure of IGF-II, it was clear that those affected by NN-BP-6 binding form a continuous surface adjacent to the C-BP-6 binding site on IGF-II determined previously (*27*) (Figure 7B). Previous studies suggest that the C-terminal domain of IGFBP-6 is a major determinant of the IGF-II binding preference of IGFBP-6 (*43*). Our results show that the binding sites for NN-BP-6 and the C-domain of IGFBP-6 on IGF-II are adjacent to one another, implying that the N- and C-domains are brought close together upon IGF binding. These observations are also consistent with the recent crystal structure of the ternary complex of N-BP-4/IGF-I/C-BP-4, which shows that the N- and C-terminal domains come into close proximity in the complex and stabilize IGF binding (*13*). The key IGF-I residues affected by NN-BP-4 are matched by corresponding residues in IGF-II affected by NN-BP-6 binding, especially Tyr27 and Phe28, which form a hydrophobic patch on IGF-II and are determinants of IGF binding to the IGF receptor (Figure 7C) (*12*, *13*). Comparison of the IGF-I/mini-BP-5 interface (*14*) with that of IGF-II/NN-BP-6 indicates that the two binding sites are adjacent to each other and the binding residues Gly10 and Gly11 on IGF-II are within two residues of the equivalent residues in IGF-I that make up the IGF-I/mini-BP-5 interface (Figure 7C).

It is evident from this study that NN-BP-6 may play a role in preferential IGF-II binding. Indeed, this flexible subdomain of IGFBP-6 may function as a recognition element for IGFs. Several studies have highlighted the significance of flexibility in protein recognition (*44*, *45*). In some proteins the flexible or intrinsically disordered regions undergo transitions to more ordered structure upon binding to their ligand by the process of coupled folding and binding (*41*), but our data show that this is unlikely for NN-BP-6. One functional advantage of the extended N-terminal subdomain of IGFBP-6 could be its ability to engage with IGF-II or other biologically relevant ligands over a larger distance than the corresponding subdomains of other IGFBPs, where the different disulfide connectivities stabilize a more compact structure. A kinetic advantage for unfolded proteins or domains in ligand binding has been postulated by the fly-casting mechanism (*44*), wherein the unfolded domain binds weakly to the ligand at a site distinct from the actual binding site over a larger distance, thereby enhancing the speed of association. This initial binding event is followed by high-affinity binding of the folded domains to the actual binding site, thus forming a tight complex. A partially structured or unstructured domain has a greater capture radius than the folded domain and can bind to the ligand with high specificity and relatively low affinity. The flexible N-terminal subdomain of IGFBP-6 could be interacting with IGFs by such a mechanism and could play a role in ligand capture and recognition of IGFs prior to high-affinity binding of the distal part of the N-domain and the proximal part of the C-domain of IGFBP-6 to IGFs. This behavior would be facilitated by the abundance of charged residues in NN-BP-6 as electrostatic interactions are effective over large distances. This mechanism of ligand recognition and binding is likely to be distinct for IGFBP-6 and unlikely to be shared by other IGFBPs because of the structural differences in the N-terminal subdomain.

Contradictory results have been reported in the literature on the contribution of the N-terminal subdomains of IGFBPs to IGF binding. An NMR study on the binding of the N-terminal domain of IGFBP-5 to IGF-II indicated that the N-terminal subdomain of IGFBP-5 did not interact with IGF-II and that this subdomain had no influence on the structure of the mini-BP-5 domain (*8*). BIAcore and ITC data showed that the K_d values for mini-BP-5 and the full-length N-terminal domain of IGFBP-5 did not differ significantly, further supporting the lack of interaction of the N-terminal subdomain of IGFBP-5 with IGFs (*12*). By contrast, it was suggested that the N-terminal subdomain of IGFBP-4 contributed to IGF-I binding and that the 4−5-fold higher affinity of the complete N-domain as compared to mini-BP-4 was a consequence of the extra contacts made by the N-terminal hydrophobic residues of NN-BP-4 with the hydrophobic patch formed by Phe23, Tyr24, and Phe25 on IGF-I (*12*). Further, it was found that the NN-BP-4 masks IGF residues responsible for IGF-IR binding, indicating a crucial role of the N-terminal subdomain of IGFBP-4 in blocking IGF activity (*12*) Truncation of the thumb region of NN-BP-4 (residues 1−5) reduced the IGF-I binding affinity of IGFBP-4, further supporting the importance of this region in IGF-I binding (*13*). Our results show that NN-BP-6 binds preferentially to IGF-II and interacts with equivalent residues of IGF-II to those observed in the N-BP-4/IGF-I/C-BP-4 ternary complex (Figure 7C). It is likely, therefore, that NN-BP-6 has a similar inhibitory effect on IGF/IGF-IR interactions. However, further mutagenesis data in the N-terminal subdomain of IGFBP-6 would be needed to quantify the inhibitory role of this domain.

NN-BP-6 forms a large binding interface with IGF-II, but it is possible that the contacts made by NN-BP-6 on the surface on IGF-II undergo some changes as the ligand engages with the full-length IGFBP-6. Whether the presence of the other high-affinity domains would weaken or strengthen the net interactions of the NN-BP-6 domain with IGF-II in the full-length IGFBP-6/IGF-II complex remains to be established. The N-terminal subdomain of IGFBP-6 is unique among the family of IGF binding proteins and appears to contribute to preferential IGF-II binding, but this subdomain may have other distinctive functions that remain to be characterized.

ACKNOWLEDGMENT

We thank Kerrie McNeil for help with the expression and purification of the labeled IGFs, Zhihe Kuang for help with assignment of IGF spectra, Jeff Babon and Jennifer Sabo for help with recording the NMR spectra and structure calculations, and Andrew Low for help with HPLC and mass spectrometry.

SUPPORTING INFORMATION AVAILABLE

NMR data referred to in the text. This material is available free of charge via the Internet at http://pubs.acs.org.

REFERENCES

1. Bach, L. A. (1999) The insulin-like growth factor system: basic and clinical aspects, *Aust. N.Z. J. Med. 29*, 355−361.
2. Yu, H., and Rohan, T. (2000) Role of the insulin-like growth factor family in cancer development and progression, *J. Natl. Cancer Inst. 92*, 1472−1489.
3. Bach, L. A., and Rechler, M. M. (1995) Insulin-like growth factor binding proteins, *Diabetes Rev. 3*, 38−61.
4. Baxter, R. C. (2000) Insulin-like growth factor (IGF)-binding proteins: interactions with IGFs and intrinsic bioactivities, *Am. J. Physiol. Endocrinol. Metab. 278*, 967−976.
5. Bach, L. A. (2005) IGFBP-6 five years on; not so 'forgotten'?, *Growth Hormone IGF Res. 15*, 185−192.
6. Bach, L. A., Headey, S. J., and Norton, R. S. (2005) IGF-binding proteins—the pieces are falling into place, *Trends Endocrinol. Metab. 16*, 228−234.
7. Neumann, G. M., and Bach, L. A. (1999) The N-terminal disulfide linkages of human insulin-like growth factor binding protein-6 (hIGFBP-6) and hIGFBP-1 are different as determined by mass spectrometry, *J. Biol. Chem. 274*, 14587−14594.
8. Kalus, W., Zweckstetter, M., Renner, C., Sanchez, Y., Georgescu, J., Grol, M., Demuth, D., Schumacher, R., Dony, C., Lang, K., and Holak, T. A. (1998) Structure of the IGF-binding domain of the insulin like growth factor-binding protein-5 (IGFBP-5): implications for IGF and IGF-I receptor interactions, *EMBO J. 22*, 6558−6572.
9. Headey, S. J., Keizer, D. W., Yao, S., Brasier, G., Kantharidis, P., Bach, L. A., and Norton, R. S. (2004) C-terminal domain of insulin-like growth factor (IGF) binding protein-6: structure and interaction with IGF-II, *Mol. Endocrinol. 18*, 2740−2750.
10. Sala, A., Capaldi, S., Campagnoli, M., Faggion, B., Labo, S., Perduca, M., Romano, A., Carrizo, M. E., Valli, M., Visai, L., Minchiotti, L., Galliano, M., and Monaco, H. L. (2005) Structure and properties of the C-terminal domain of insulin-like growth factor-binding protein-1 isolated from human amniotic fluid, *J. Biol. Chem. 280*, 29812−29819.
11. Kuang, Z., Yao, S., Keizer, D. W., Wang, C. C., Bach, L. A., Forbes, B. E., Wallace, J. C., and Norton, R. S. (2006) Structure, dynamics and heparin binding of the C-terminal domain of insulin-like growth factor binding protein-2 (IGFBP-2), *J. Mol. Biol. 364*, 690−704.
12. Siwanowicz, I., Popowicz, G. M., Wisniewska, M., Huber, R., Kuenkele, K. P., Lang, K., Engh, R. A., and Holak, T. A. (2005) Structural basis for the regulation of insulin-like growth factors by IGF binding proteins, *Structure 13*, 155−167.
13. Sitar, T., Popowicz, G. M., Siwanowicz, I., Huber, R., and Holak, T. A. (2006) Structural basis for the inhibition of insulin-like growth factors by insulin-like growth factor-binding proteins, *Proc. Natl. Acad. Sci. U.S.A. 103*, 13028−13033.
14. Zesławski, W., Beisel, H. G., Kamionka, M., Engh, R. A., Huber, R., Lang, K., and Holak, T. A. (2001) The interaction of insulin-like growth factor-I with the N-terminal domain of IGFBP-5, *EMBO J. 20*, 3638−3644.
15. Sackett, R. L., and McCusker, R. H. (1998) Multivalent cations depress ligand affinity of insulin-like growth factor-binding proteins-3 and -5 on human GM-10 fibroblast cell surfaces, *J. Cell. Biochem. 69*, 364−375.
16. Sackett, R. L., and McCusker, R. H. (1998) Multivalent cations depress ligand binding to cell-associated insulin-like growth factor binding protein-5 on human glioblastoma cells, *Endocrinology 139*, 1943−1951.
17. Bax, A., Griffey, R. H., and Hawkins, B. L. (1983) Correlation of proton and N-15 chemical shifts by multiple quantum NMR, *J. Magn. Reson. 55*, 301−315.
18. Bax, A., and Grzesiek, S. (1993) Methodological advances in protein NMR, *Acc. Chem. Res. 26*, 131−138.
19. Yao, S., Howlett, G. J., and Norton, R. S. (2000) Peptide self-association in aqueous trifluoroethanol monitored by pulsed field gradient NMR diffusion measurements, *J. Biomol. NMR 16*, 109−119.
20. Wishart, D. S., Bigam, C. G., Yao, J., Abildgaard, F., Dyson, H. J., Oldfield, E., Markley, J. L., and Sykes, B. D. (1995) ^{1}H, ^{13}C and ^{15}N chemical shift referencing in biomolecular NMR, *J. Biomol. NMR 6*, 135−140.
21. Bartels, C., Xia, T., Billeter, M., Güntert, P., and Wüthrich, K. (1995) The program XEASY for computer-supported NMR spectral analysis of biological macromolecules, *J. Biomol. NMR 6*, 1−10.
22. Herrmann, T., Güntert, P., and Wüthrich, K. (2002) Protein NMR structure determination with automated NOE assignment using the new software CANDID and the torsion angle dynamics algorithm DYANA, *J. Mol. Biol. 319*, 209−227.
23. Schwieters, C. D., Kuszewski, J. J., Tjandra, N., and Clore, G. M. (2003) The X-PLOR-NIH NMR molecular structure determination package, *J. Magn. Reson. 160*, 65−73.
24. Laskowski, R. A., Rullmann, J. A., MacArthur, M. W., Kaptein, R., and Thornton, M. (1996) AQUA and PROCHECK-NMR: programs for checking the quality of protein structures solved by NMR, *J. Biomol. NMR 8*, 477−486.
25. Koradi, R., Billeter, M., and Wüthrich, K. (1996) MOLMOL: a program for display and analysis of macromolecular structures, *J. Mol. Graphics 14*, 51−55.
26. Torres, A. M., Forbes, B. E., Aplin, S. E., Wallace, J. C., Francis, G. L., and Norton, R. S. (1995) Solution structure of human insulin-like growth factor II. Relationship to receptor and binding protein interactions, *J. Mol. Biol. 248*, 385−401.
27. Headey, S. J., Keizer, D. W., Yao, S., Wallace, J. C., Bach, L. A., and Norton, R. S. (2004) Binding site for the C-domain of insulin-like growth factor (IGF) binding protein-6 on IGF-II; implications for inhibition of IGF actions, *FEBS Lett. 568*, 19−22.
28. Otting, G., and Wüthrich, K. (1989) Extended heteronuclear editing of 2D H-1-NMR spectra of isotope-labeled proteins, using the X (ω_1 ω_2) double half filter, *J. Magn. Reson. 85*, 586−594.
29. Pellecchia, M., Sebbel, P., Hermanns, U., Wüthrich, K., and Glockshuber, R. (1999) Pilus chaperone FimC-adhesin FimH interactions mapped by TROSY-NMR, *Nat. Struct. Biol. 6*, 336−339.
30. Klaus, W., Broger, C., Gerber, P., and Senn, H. (1993) Determination of the disulphide bonding pattern in proteins by local and global analysis of nuclear magnetic resonance data. Application to flavoridin, *J. Mol. Biol. 232*, 897−906.
31. Sabo, J. K., Keizer, D. W., Feng, Z. P., Casey, J. L., Parisi, K., Coley, A. M., Foley, M., and Norton, R. S. (2007) Mimotopes of apical membrane antigen 1: structures of phage-derived peptides recognized by the inhibitory monoclonal antibody 4G2dc1 and design of a more active analogue, *Infect. Immun. 75*, 61−73.
32. Keizer, D. W., Miles, L. A., Li, F., Nair, M., Anders, R. F., Coley, A. M., Foley, M., and Norton, R. S. (2003) Structures of phage-display peptides that bind to the malarial surface protein, apical membrane antigen 1, and block erythrocyte invasion, *Biochemistry 42*, 9915−9923.
33. Bertini, I., Donaire, A., Jimenez, B., Luchinat, C., Parigi, G., Piccioli, M., and Poggi, L. (2001) Paramagnetism-based versus classical constraints: an analysis of the solution structure of Ca Ln calbindin D9k, *J. Biomol. NMR 21*, 85−98.
34. Lee, L., and Sykes, B. D. (1983) Use of lanthanide-induced nuclear magnetic resonance shifts for determination of protein structure in solution: EF calcium binding site of carp parvalbumin, *Biochemistry 22*, 4366−4373.
35. Bertini, I., Luchinat, C., Parigi, G., and Pierattelli, R. (2005) NMR spectroscopy of paramagnetic metalloproteins, *ChemBioChem 6*, 1536−1549.
36. Denley, A., Wang, C. C., McNeil, K. A., Walenkamp, M. J., van Duyvenvoorde, H., Wit, J. M., Wallace, J. C., Norton, R. S., Karperien, M., and Forbes, B. E. (2005) Structural and functional characteristics of the Val44Met insulin-like growth factor I missense mutation: correlation with effects on growth and development, *Mol. Endocrinol. 19*, 711−721.
37. Huang, X., Yang, X., Luft, B. J., and Koide, S. (1998) NMR identification of epitopes of Lyme disease antigen OspA to monoclonal antibodies, *J. Mol. Biol. 281*, 61−67.
38. Ding, W., Huang, X., Yang, X., Dunn, J. J., Luft, B. J., Koide, S., and Lawson, C. L. (2000) Structural identification of a key protective B-cell epitope in Lyme disease antigen OspA, *J. Mol. Biol. 302*, 1153−1164.
39. Fielding, L. (2003) NMR methods for the determination of protein-ligand dissociation constants, *Curr. Top. Med. Chem. 3*, 39−53.
40. Dunker, A. K., Lawson, J. D., Brown, C. J., Williams, R. M., Romero, P., Oh, J. S., Oldfield, C. J., Campen, A. M., Ratliff, C. M., Hipps, K. W., J., A., Nissen, M. S., Reeves, R., Kang, C., Kissinger, C. R., Bailey, R. W., Griswold, M. D., Chiu, W.,

Garner, E. C., and Obradovic, Z. (2001) Intrinsically disordered protein, *J. Mol. Graphics Modell. 19*, 26−59.
41. Dyson, H. J., and Wright, P. E. (2005) Intrinsically unstructured proteins and their functions, *Nat. Rev. Mol. Cell Biol. 6*, 197−208.
42. Jonker, H. R., Wechselberger, R. W., Boelens, R., Kaptein, R., and Folkers, G. E. (2006) The intrinsically unstructured domain of PC4 modulates the activity of the structured core through inter- and intramolecular interactions, *Biochemistry 45*, 5067−5081.
43. Headey, S. J., Leeding, K. S., Norton, R. S., and Bach, L. A. (2004) Contributions of the N- and C-terminal domains of IGF binding protein-6 to IGF binding, *J. Mol. Endocrinol. 33*, 377−386.
44. Shoemaker, B. A., Portman, J. J., and Wolynes, P. G. (2000) Speeding molecular recognition by using the folding funnel: the fly-casting mechanism, *Proc. Natl. Acad. Sci. U.S.A. 97*, 8868−8873.
45. Levy, Y., Cho, S. S., Onuchic, J. N., and Wolynes, P. G. (2005) A survey of flexible protein binding mechanisms and their transition states using native topology based energy landscapes, *J. Mol. Biol. 346*, 1121−1145.
46. Merutka, G., Dyson, H. J., and Wright, P. E. (1995) "Random coil" ^{1}H chemical shifts obtained as a function of temperature and trifluoroethanol concentration for the peptide series GGXGG, *J. Biomol. NMR 5*, 14−24.

BI0619876